Philosophical Magazine

ISSN: 1478-6435 (Print) 1478-6443 (Online) Journal homepage: http://www.tandfonline.com/loi/tphm20

Deformation mechanisms of ultra-thin Al layers in Al/SiC nanolaminates as a function of thickness and temperature

L. W. Yang, C. Mayer, N. Chawla, J. Llorca & J. M. Molina-Aldareguía

To cite this article: L. W. Yang, C. Mayer, N. Chawla, J. Llorca & J. M. Molina-Aldareguía (2016): Deformation mechanisms of ultra-thin Al layers in Al/SiC nanolaminates as a function of thickness and temperature, Philosophical Magazine, DOI: 10.1080/14786435.2016.1219075

To link to this article: http://dx.doi.org/10.1080/14786435.2016.1219075

Published online: 16 Aug 2016.

PHILOSOPHICAL MAGAZINE, 2016
http://dx.doi.org/10.1080/14786435.2016.1219075

Taylor & Francis
Taylor & Francis Group

Deformation mechanisms of ultra-thin Al layers in Al/SiC nanolaminates as a function of thickness and temperature

L. W. Yang[a], C. Mayer[c], N. Chawla[c], J. Llorca[a,b] and J. M. Molina-Aldareguía[a]

[a]IMDEA Materials Institute, Madrid, Spain; [b]Department of Materials Science, Polytechnic University of Madrid, Madrid, Spain; [c]Materials Science and Engineering, Arizona State University, Tempe, AZ, USA

ABSTRACT

The mechanical properties of Al/SiC nanolaminates with layer thicknesses between 10 and 100 nm were studied by nanoindentation in the temperature range 25 to 100 °C. The strength of the Al layers as a function of the layer thickness and temperature was obtained from the hardness of the nanolaminates by an inverse methodology based on the numerical simulation of the nanoindentation tests by means of the finite element method. The room temperature yield stress of the Al layers showed a large 'the thinner, the stronger' effect, which depended not only on the layer thickness but also on the microstructure, which changed with the Al layer thickness. The yield stress of the Al layers at ambient temperature was compatible with a deformation mechanism controlled by the interaction of dislocations with grain boundaries for the thicker layers (>50 nm), while confined layer slip appeared to be dominant for layers below 50 nm. There was a dramatic reduction in the Al yield stress with temperature, which increased as the Al layer thickness decreased, and led to an inverse size effect at 100 °C. This behavior was compatible with plastic deformation mechanisms controlled by grain boundary and interface diffusion at 100 °C, which limit the strength of the ultra-thin Al layers.

ARTICLE HISTORY
Received 5 November 2015
Accepted 26 July 2016

KEYWORDS
Multilayers; nanoindentation; thin-films; finite element modeling

1. Introduction

Nanolaminates consisting of alternating layers of two dissimilar materials show outstanding mechanical properties, as compared to their bulk counterparts, and they are very promising for engineering applications [1–20]. In particular, extremely high strength and damage tolerance have been reported at ambient temperature when the individual layer thicknesses are below 100 nm, and this behavior has been attributed to the large density of interfaces and to the nanoscale layer dimensions. The deformation behavior, though, is dependent on the particular nature of the layers in the nanolaminate. The mechanical behavior of nanolaminates has been extensively studied in metallic systems, such as Cu/Ni [21], Cu/Au [20], Cu/Nb [4,7,11,18,19,22], Cu/W [2,12], Cu/Zr [9], Al/Nb [3], etc. Both metallic layers deform plastically in response to the applied stress and the hardening mechanisms

CONTACT J. M. Molina-Aldareguía jon.molina@imdea.org

are controlled by the interaction between dislocations and interfaces [20–22]. These investigations have shown that the strengthening follows a Hall-Petch behavior when the layer thickness is in the sub-micrometer range due to the pinning of dislocations by interfaces/grain boundaries, giving rise to the formation of dislocation pile-ups [14–17]. For layer thicknesses in the range of a few tens of nm, plastic deformation is controlled by confined layer slip (CLS) [17–19], because of the impossibility to accommodate more than one dislocation along the layer thickness.

Metallic crystalline-amorphous nanolaminates, such as Cu/CuZr [8] and Cu/PdSi [10] also present very high strengths. The amorphous-crystalline interface can be regarded as an impenetrable barrier for dislocations, and previous studies suggest that initiation of plasticity takes place in the softer metallic layers [10], followed by a marked strain hardening attributed to dislocation multiplication. Co-deformation of the amorphous layers can be triggered at very high stresses through the formation of shear bands, which can propagate or remain confined, depending on the relative layer thickness ratio [8].

Different hardening mechanisms have been reported, however, in metal-ceramic nanolaminates [6,13,17,23–31]. Co-deformation of the layers is much more difficult because of large mismatch in the elastic modulus and flow stress between the stiff, brittle ceramic layer and the softer and ductile metallic layer. Under these conditions, multilayer deformation is concentrated in the metallic layers, which show very large plastic strain hardening rates, while the ceramic layers remain elastic or fracture, depending on the applied strain and layer thickness [23,25–27]. Detailed numerical simulations [25,27] have demonstrated that the large strain hardening of the metal-ceramic nanolaminates is not due to the multiplication of dislocations in the metallic layers, but can be attributed to build up of hydrostatic stresses due the elastic constraint imposed by the ceramic layers to the metallic layers plastic flow [32,33].

Thus, the available experimental information shows that the yield stress of ultra-thin (<100 nm) metallic layers within nanolaminate composites is extremely high. However, quantitative data of the yield stress of the individual layers as a function of the layer thickness is very limited [34] and the effect of temperature on the strength of ultra-thin metallic layers has not been explored. This quantitative information can be very useful to understand the dominant deformation mechanisms in each nanolaminate system as well as to explore the role played by grain boundary/interface diffusion during high temperature deformation.

This investigation contributed to these goals by providing an estimation of the yield stress of the Al nanolayers as a function of the layer thickness and temperature (in the range 25 to 100 °C) in Al/SiC nanolaminates. The yield stress of the Al nanolayers was obtained following an inverse methodology from the numerical simulation of the nanoindentation response of the nanolaminate. This Al/SiC nanolaminate system is ideally suited for this approach because previous work [23–28] has shown that the (amorphous) SiC nanolayers undergo elastic deformation and their mechanical properties are independent of the temperature up to 300 °C [29,31]. Moreover, the strength of the SiC layers seems to be independent of layer thickness, at least for layers as thin as 25 nm [31], in agreement with what has been observed for other amorphous ultra-thin layers like PdSi [10]. Using the inverse methodology, the yield stress of the Al nanolayers with thickness in the range 10 to 100 nm was obtained from ambient temperature to 100 °C from nanoindentation tests carried out in nanolaminates in which the SiC layer thickness was kept constant and equal to 50 nm. These values of the yield stress were validated by comparing the numerical predictions of the nanoindentation

hardness with the experimental results obtained in other set of nanolaminates in which the thickness of Al and SiC layers was the same (between 10 and 100 nm). Finally, the quantitative values of the yield stress of the Al nanolayers as a function of temperature and layer thickness were used to ascertain the dominant deformation mechanisms in light of the current theories for plastic deformation of ultra-thin metallic films.

2. Materials and experimental techniques

2.1. Al/SiC nanolaminate fabrication and microstructural characterization

The Al/SiC nanolaminates were manufactured by magnetron sputtering of Al and SiC in Los Alamos National Laboratory using a sputter unit made up of a high vacuum chamber with dual sputter guns. Thermally oxidized (111) oriented single crystal silicon (Si) wafers were used as substrates. The base pressure of the sputtering unit was 10^{-7} Torr. Argon (Ar) was used as the sputter gas and all depositions were carried out at an Ar working pressure of 3.0 m Torr (0.4 Pa). The pure aluminum target (>99.99% purity, Kurt J. Lesker, Clairton, PA) was sputtered at a DC power of 95 W. SiC layers were deposited from a SiC target made by hot isostatic pressing (>99.5% purity, Kurt J. Lesker, Clairton, PA) using identical argon pressure and a RF sputter power of 215 W. The targets were pre-sputtered for about 10 min at 40 W for Al and 95 W for SiC to remove any oxides and contamination prior to nanolaminate deposition. The sample holder was continuously rotated during sputtering to obtain a uniform layer thickness. The deposition rates were approximately 7.5 nm/min for Al and 3.9 nm/min for SiC. Alternating Al and SiC layers were deposited by means of a computer controlled shutter system to build up the multilayer structure.

Two nanolaminate series (named series I and II) were manufactured. In series I, the nominal SiC layer thickness was kept constant at 50 nm and the nominal Al layer thickness was varied between 10 and 100 nm. In series II, both the Al and SiC layers were grown to the same thickness and the nominal layer thickness was varied between 10 and 100 nm. The total number of layers in each nanolaminate was chosen to obtain a total thickness above 10 μm to reduce substrate effects during nanoindentation. Note that the convention used to name each nanolaminate refers to the nominal thickness, in nm, of each layer, but that the real thicknesses might vary. In order to build a realistic FEM model for each nanolaminate, the average layer thicknesses and the average grain size of the Al layers were measured by transmission electron microscopy (TEM) using a JEOL JEM 2100 microscope.

2.2. High temperature nanoindentation

Nanoindentation tests were carried out using a NanoTest™ platform III (Micro Materials, Wrexham, UK) with a Berkovich diamond tip. Nanoindentation tests were performed at 25, 50 and 100 °C. Samples were bonded to the heater plate using a high temperature adhesive and then both sample and indenter were heated independently to the target temperature. Indentations were carried out with a loading rate of 10 mN/s and a maximum load of 100 mN. The maximum load was held constant for a dwell period of 5 s prior to unloading with 20 mN/s. The measured thermal drift was lower than 0.01 nm/s in all cases. The total penetration depth was carefully controlled within 1 μm, less than 10% of the total nanolaminate thickness to eliminate substrate effects. This penetration depth was also set deep

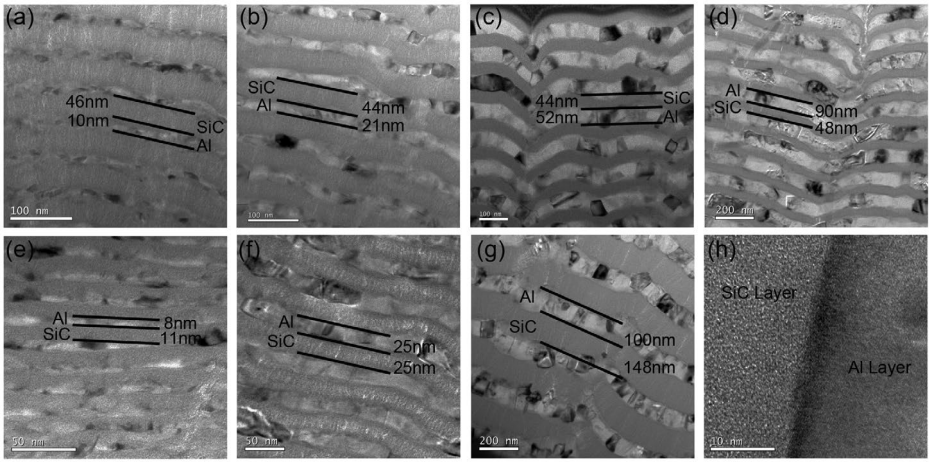

Figure 1. BF-TEM images of series I samples: (a) Al10SiC50, (b) Al25SiC50, (c) Al50SiC50, (d) Al100SiC50. BF-TEM of series II samples: (e) Al10SiC10, (f) Al25SiC25, (g) Al100SiC100; (h) HR-TEM of Al100SiC100.

enough compared to the individual layer thickness, to obtain the overall nanolaminate response. At least 8 indentations were performed at each temperature. The load-penetration curves after nanoindentation were analyzed using the Oliver and Pharr method [35]. Selected indents were cross-sectioned with a FEI Helios Nanolab 600i dual-beam system to analyze the deformation patterns in the TEM.

3. Experimental results and discussion

3.1. Microstructure of as-deposited nanolaminates

Figure 1(a)–(h) shows bright field cross sectional TEM (BF-TEM) and high resolution TEM (HR-TEM) images of series I and II samples. All samples presented a chemically modulated layered structure, with the Al and SiC growing with nanocrystalline and amorphous structure, respectively. The SiC layers, due to their amorphous nature, interrupted the crystalline growth of each Al layer, forcing the next Al layer to re-nucleate. As a result, the Al layers presented a nanocolumnar grain structure where the vertical, columnar grain size, d_v, was equal to the layer thickness, h_{Al}. Interestingly, the lateral grain size, d_l, scaled with the layer thickness but did not follow a constant relation with it, as shown in Table 1. The lateral grain size was larger than the layer thickness for Al layer thicknesses below 25 nm, while it was smaller than the layer thickness for thicknesses above 50 nm. For instance, the 10 nm thick Al layers showed a lateral grain size of ≈30 nm, irrespective of the thickness of the SiC layers (compare Al10SiC50 and Al10SiC10). This result indicates that the Al grains nucleated on each consecutive SiC layer grew quickly up to 30 nm in the in-plane orientation, and that the nucleation process on top of each consecutive amorphous SiC layer was independent of its thickness. As the Al layer thickness increased, columnar growth proceeded and the grains experienced some lateral grain growth at a rate smaller than the increase in thickness. As a result, the aspect ratio of the Al grains changed at 50 nm, with the vertical dimension becoming longer than the lateral grain size. The Al layers displayed a random texture in the thickness range studied. Figure 1(a)–(g) also shows that the Al-SiC interfaces developed

Table 1. Average thickness of Al and SiC layers in series I and II nanolaminates, as measured from TEM.

Series	Nanolaminate	Thickness	Layer thickness		Al grain size		V_{Al}
		μm	h_{Al} (nm)	h_{SiC} (nm)	vertical, d_v (nm)	lateral, d_l (nm)	(%)
Series I	Al10SiC50	~15	10 ± 1	46 ± 3	10 ± 1	29 ± 5	~17.9
	Al25SiC50	~13.3	21 ± 1	44 ± 2	21 ± 1	47 ± 12	~32.3
	Al50SiC50	~15	52 ± 2	44 ± 2	52 ± 2	48 ± 7	~54.2
	Al100SiC50	~15	90 ± 8	48 ± 3	90 ± 8	65 ± 12	~64.3
Series II	Al10SiC10	~12	8 ± 1	11 ± 2	8 ± 1	29 ± 6	~42.1
	Al25SiC25	~14	25 ± 4	25 ± 7	25 ± 4	47 ± 11	~50
	Al100SiC100	~17	100 ± 6	148 ± 5	100 ± 6	62 ± 12	~40.8

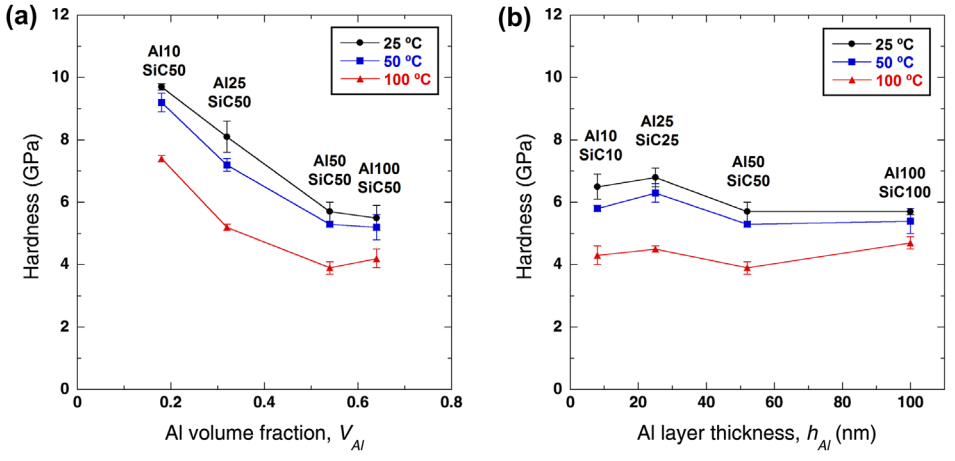

Figure 2. (colour online) (a) Hardness of series I nanolaminates as a function of the Al volume fraction, V_{Al}. (b) Hardness of series II nanolaminates as a function of the Al layer thickness, h_{Al}.

some waviness as a result of the competitive columnar grain growth process that takes place in each consecutive Al layer [27]. No formation of secondary phases or intermixing could be found at the Al-SiC interfaces, as shown in the HR-TEM image of Figure 1(h). Finally, even though the Al and SiC layers were relatively uniform in thickness, the actual thicknesses measured in the BF-TEM micrographs were slightly different from the nominal ones, as reported in Table 1.

3.2. Ambient and elevated temperature hardness

The hardness of Al/SiC is known to vary with the volume fraction of the constituents and the strength of each individual layer [31]. The hardness of the nanolaminates is plotted in Figure 2(a) and (b) as a function of Al volume fraction, V_{Al}, and of Al layer thickness, h_{Al}, respectively, in the temperature range 25–100 °C. The hardness of the series I nanolaminates (constant SiC layer thickness) in Figure 2(a) increased nonlinearly as the Al volume fraction decreased. In contrast, previous work on nanolaminates with constant Al thickness and varying SiC thickness [31] showed a linear increase of hardness as Al volume fraction decreased. This difference implies that the strength of the Al layers depends on the layer thickness, because of their nanocrystalline microstructure, while the strength of the amorphous SiC layers is size independent [28]. The nanoindentation tests of the series II nanolaminates

confirmed this hypothesis: the hardness increased as the layer thickness decreased at a constant Al volume fraction of 50%, reaching a peak for a layer thickness of 25 nm (Figure 2(b)). This behavior is similar to that reported in other metal-ceramic nanolaminates like Ti/TiN, Hf/HfN or W/WN [36]. It is worth noting that the Al100SiC100 and Al50SiC50 nanolaminates showed similar hardness, and this may be due to the fact that the critical dimension controlling the strength was the lateral grain size, which was also similar in both nanolaminates and smaller than the layer thickness (Table 1). Interestingly, the trend was not maintained for the Al10SiC10 nanolaminate, suggesting that other deformation mechanisms and/or microstructural changes may be triggered when both layers are reduced to this extremely small scale. The reasons for this behavior will be discussed later in more detail.

The nanolaminate hardness experienced a significant reduction with temperature, as shown in Figure 2, which was more marked for the thinner nanolaminates. According to micropillar compression tests in Al50SiC50 [27,28], the reduction in strength with temsperature could be attributed to a reduction in the Al yield stress and to the development of interface sliding at the Al-SiC interface. The contribution of Al-SiC interface sliding to the high temperature deformation of micropillars [27] was evidenced by extrusion of Al grains out of the free edges of the micropillar. However, the lack of free surfaces and the constraint imposed by the surrounding undeformed material renders unlikely that interface sliding might contribute to a large extent to the deformation in the case of nanoindentation. In addition, it is also unlikely that the mechanical properties of the SiC layers experience any softening at 100 °C. Thus, it was assumed that the hardness drop with temperature of the Al/SiC nanolaminates was a direct consequence of the reduction in the yield stress of the Al layers. It should be noted that 100 °C represents a homologous temperature of 0.4 for Al, high enough to activate dislocation climb and/or interface and grain boundary diffusion. These mechanisms can lead to a marked softening of the nanocrystalline Al layers, beyond to what it would be expected only by the reduction of shear modulus with temperature.

Electron-transparent lamellae across indents were prepared by focus ion beam milling after nanoindentation at different temperatures and examined by TEM. Figure 3(a)–(c) show representative TEM images of the indents carried out at room temperature for nanolaminates layer thicknesses of 100, 25 and 10 nm, respectively. The layered structure was preserved in all cases, with no evidence of interface fracture or interface sliding. It is clear that the deformation of the Al layers was severely constrained by the hard SiC layers [37], especially under the indentation imprints where the imposed strains are more severe, as evidenced by the large reduction in Al layer thickness. The reduction of the Al layer thickness was accompanied by a change in grain shape, which grew parallel to the layers, as shown by the white arrows. This indicates that plastic deformation processes took place not only at interfaces or grain boundaries, but also within the grains. However, not a single dislocation could be observed in the deformed layers, suggesting that the deformation is either not due to dislocation motion or that the small grain size precludes any storage of dislocations, that annihilate either at grain boundaries and/or interfaces after slipping across the grain. Thus, it should be emphasized that the dislocation density within the deformed layers remains extremely low and the large apparent strain hardening usually found in Al/SiC multilayers cannot be due to dislocation storage within the metallic layers but to the constraint imposed by the stiff ceramic layers on the plastic deformation of the metallic layers [27]. This statement might not hold true for other metal ceramic nanolaminates, like Al-TiN [38], where high strain hardening rates have been associated with plastic co-deformation of the two

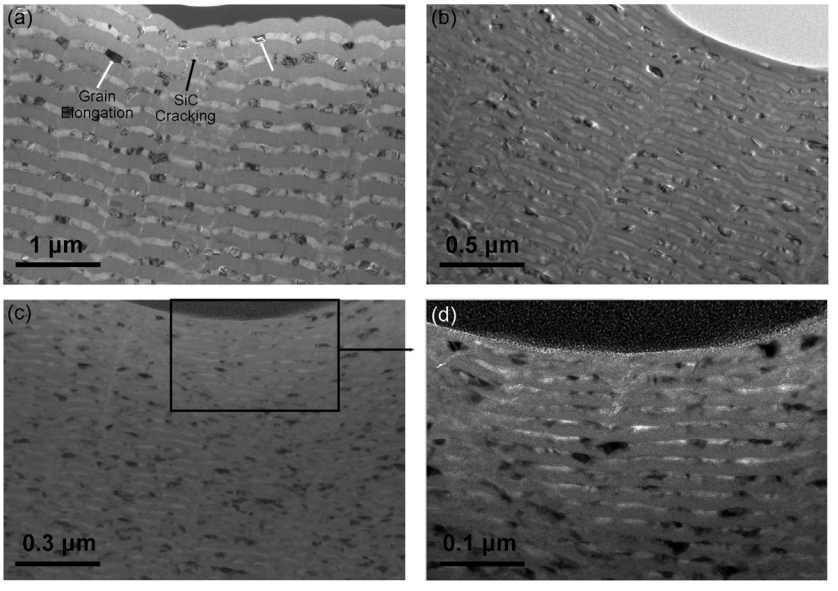

Figure 3. BF-TEM images of series II nanolaminates after room temperature nanoindentation: (a) Al100SiC100, (b) Al25SiC25, (c,d) Al10SiC10.

layers when the ceramic layers become extremely thin. No evidence of such effects have been found, however, in the case of Al/SiC nanolaminates.

As opposed to the Al layers, the SiC layers did not undergo large thickness reductions but they deformed permanently to accommodate the indenter shape. Despite the brittle nature of SiC, some plastic deformation cannot be ruled out due to the large hydrostatic stresses imposed below the indenter. Some cracking of the SiC layers is evident, especially for the thicker layers in Al100SiC100, as pointed by the black arrows in Figure 3(a). Cracks are perpendicular to the layers as a result of the bending stresses and provide paths where the Al can plastically flow during deformation. The extent of cracking of the SiC layers was reduced for the thinner SiC layers (Al25SiC25 and Al10SiC10), as a result of their larger bending compliance and to their enhanced ductility (Figure 3(b)–(d)) [23]. In any case, cracking of the SiC layers was not the major mechanism accommodating the imprint imposed by the indenter and was not further considered to build the numerical model.

4. Inverse methodology

The experimental results presented above indicate that the hardness of Al/SiC nanolaminates is mainly controlled by the composite response of the constituents. It is reasonable to assume that the strength of the amorphous SiC layers was independent of the layer thickness and temperature, at least up to 100 °C. Therefore, the experimental variation of the nanolaminate hardness with layer thickness and temperature has to be attributed to changes in the Al yield stress and/or the Al/SiC interfaces. Previous micropillar compression studies [26] showed that interface sliding might be triggered at the free surface of the pillar at elevated temperature, reducing the level of constraint imposed by the SiC layers. However, in the case of nanoindentation, the constraint imposed by the surrounding undeformed material

yields unnecessary to consider interface sliding as a potential deformation mechanism. Under these hypotheses, it is possible to obtain the yield stress of the Al layers from the nanolaminate response using an inverse methodology based on the numerical simulation of the nanoindentation experiments with the finite element method. This phenomenological model attributes all hardness changes to changes in the flow stress of the Al layers with layer thickness and temperature, without making any assumptions on the operating deformation mechanisms. In order to validate the approach of the inverse methodology, the mechanical response provided by the numerical model (in terms of hardness) as first fitted with the experimental results for series I nanolaminates at 25, 50 and 100 °C. And the accuracy of the quantitative data determined for the Al yield stress was then assessed by comparing the predictions of the numerical model with the experimental results of series II nanolaminates at different temperatures.

4.1. Numerical model

The numerical simulations of the nanoindentation experiments were performed using the finite element method with the commercial software Abaqus 6.13. The axisymmetric 2D model is depicted in Figure 4(a). It includes the Al/SiC nanolaminate with 10 μm in thickness (similar to the real nanolaminate thickness and with the top layer of SiC), the Si substrate and the rigid conical indenter. The lateral dimensions of the model were large enough to avoid any boundary effects. The indenter semi-angle was 70.3°, resulting in the same projected area as that of a Berkovich indenter [39]. The actual average layer thickness measured by TEM (Table 1) was used in each case, leading to seven different models to represent the nanolaminates in series I and II (Figure 4(b)). The waviness of the layers was not explicitly included in the models because it does not influence the hardness when the indentation is perpendicular to the layers [40, 41].

The model was discretized using two-dimensional four-node linear axisymmetric elements with reduced integration (CAX4R) and the mesh was refined around the upper-left corner. It was checked that the mesh used in the simulations was fine enough to provide results independent of the element size. The boundary conditions were consistent with the axial symmetry of the model: the horizontal displacement of the left boundary was impeded while the bottom boundary was fully constrained in both the horizontal and vertical directions. The remaining surfaces were unconstrained. The indenter was represented by a rigid surface. The friction coefficient between the nanolaminate and the indenter was 0.1.

The Al and SiC were modeled as isotropic, elasto-plastic solids, with no strain hardening, following the J2 theory of plasticity. This was chosen as a compromise to limit the number of parameters to determine from the inverse analysis, but has been proven to yield reasonable results in previous micropillar compression studies in the same material [26]. Si was modeled as an isotropic, elastic solid. The elastic modulus and Poisson's ratio of all three materials were obtained from literature [27] and are listed in Table 2. Even though SiC is a brittle material, it undergoes plastic deformation under the indent due to the high compressive hydrostatic stresses. The yield stress of SiC was 7 GPa, as estimated from the nanoindentation response of 1 μm thick monolithic SiC films. It was assumed constant and independent of SiC layer thickness and temperature. The Al yield stress was varied in the range 0.2 to 1.6 GPa because this was the range expected for the yield stress of the Al nanolayers in the temperature range under study.

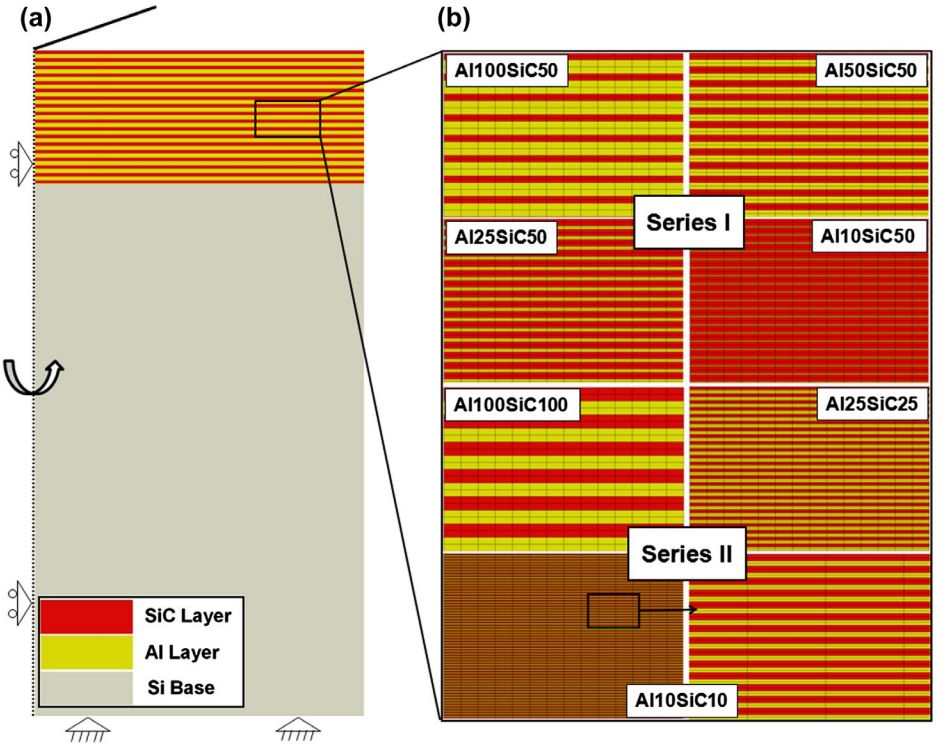

Figure 4. (colour online) (a) Schematic of finite element models to simulate nanoindentation of the Al/SiC nanolaminates. (b) Model structures of series I nanolaminates (Al100SiC50, Al50SiC50, Al25SiC50, Al10SiC50) and series II nanolaminates (Al100SiC100, Al25SiC25, Al10SiC10).

Table 2. Elastic constants of Al, SiC and Si considered in the numerical models.

Material	Elastic modulus (GPa)	Poisson's ratio
Al	70	0.34
SiC	300	0.14
Si	187	0.28

The maximum penetration of the indenter was set to 1 μm in all cases and the hardness was obtained from the simulated load-penetration curves from the Oliver and Pharr method [35], following the same procedure as in the experimental work. Simulations were carried out using Abaqus/Standard within the framework of the finite deformations theory with the initial unstressed state as reference.

4.2. Numerical results and determination of the Al yield stress

Representative load-penetration curves obtained from the numerical simulations of the Al50SiC50 nanolaminate are plotted in Figure 5 for different values of the Al yield stress. They show that the nanolaminate deformation was very sensitive to the Al flow stress although the deformation mechanisms did not change. The contour plots of the accumulated plastic strain, $\overline{\varepsilon}_p$, in the Al50SiC50 nanolaminate at the maximum indentation depth of

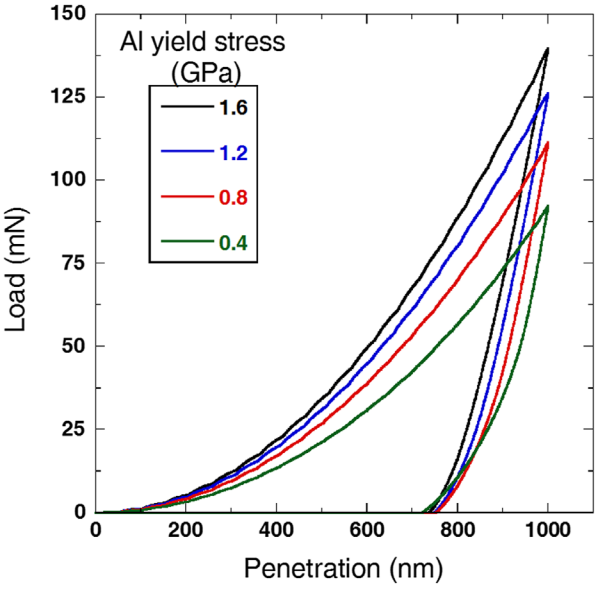

Figure 5. (colour online) Load-penetration curves obtained from the numerical simulation of the Al50SiC50 nanolaminate as a function of Al yield stress.

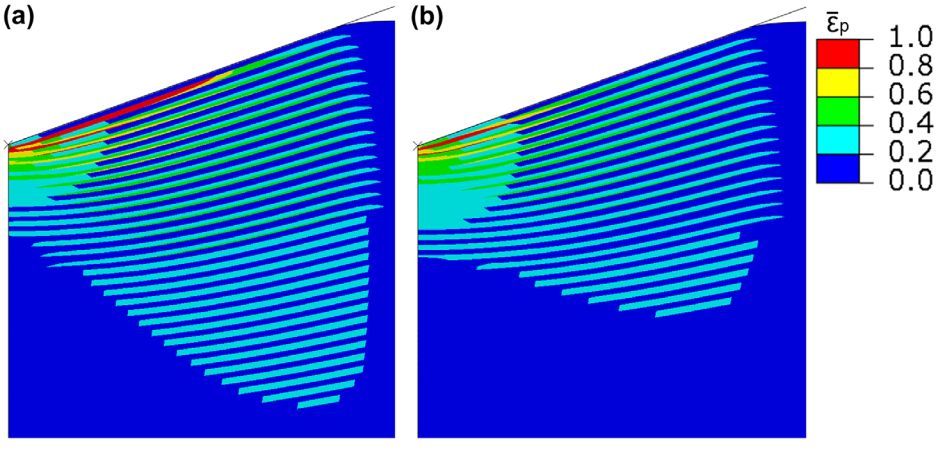

Figure 6. (colour online) Contour plot of the accumulated plastic strain in the Al50SiC50 nanolaminate at the maximum indentation depth of 1 μm. (a). Al yield stress of 0.4 GPa. (b) Al yield stress of 1.4 GPa.

1 μm are shown in Figure 6(a) and (b) for Al yield stresses of 0.4 and 1.4 GPa, respectively. The plastic zone was confined below the contact area in both cases and it was localized in the Al layers. Plastic deformation of the SiC layers only occurred in a very small region encompassing two or three SiC layers under the indenter. Pile-up formation around the indenter was not observed, and this confirmed the validity of the Oliver and Pharr method to compute the hardness.

The hardness of the series I nanolaminates as a function of Al yield stress obtained from the numerical simulations is plotted in Figure 7(a). The hardness scaled linearly with the Al

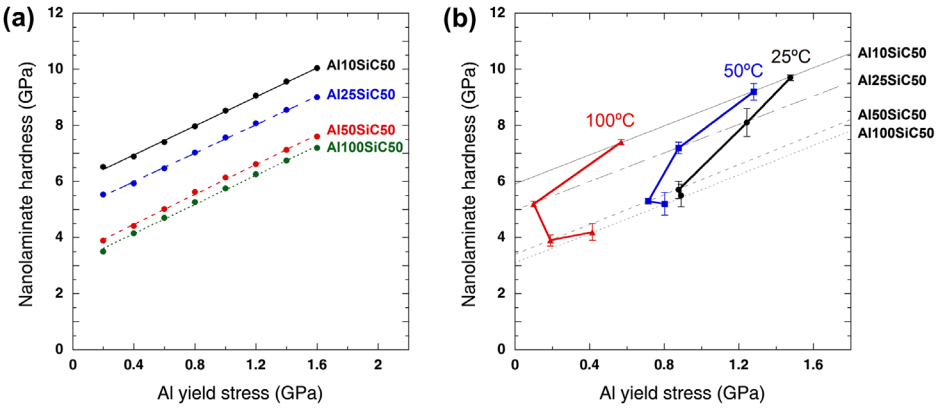

Figure 7. (colour online) (a) Master curves of the influence of the Al yield stress on the hardness of series I nanolaminates obtained from numerical simulations. (b) Determination of Al yield stress as a function of the layer thickness and temperature from the master curves and the experimental values of the hardness of series I nanolaminates.

yield stress and the slope was independent of the Al volume fraction in the nanolaminate and around ≈2.7, which is remarkably close to the Tabor factor between hardness and yield stress in metals [38].

The master curves in Figure 7(a) were the foundation of the inverse methodology to obtain the yield stress of Al as a function of the layer thickness and temperature from the experimental values of the hardness, based only on the experimental hardness measured on the nanolaminates of series I (with a constant SiC layer thickness). In this figure, the solid symbols stand for the experimental hardness at different temperatures, which are plotted on top of the master curves obtained from the numerical simulations. The corresponding abscissa in Figure 7(b) provides the quantitative value of the Al yield stress to attain the experimental hardness according to the numerical simulations. The estimations of the Al yield stress as a function of actual Al layer thickness (measured in the TEM images) and temperature are depicted in Table 3. At room temperature, the yield stress of the Al layers was much higher for thinner layers, in agreement with 'the thinner, the stronger' effect. This size effect on the yield stress disappears, however, at 100 °C because the reduction in the yield stress with temperature was much more dramatic for the thinner Al layers.

4.3. Validation of the yield stress obtained by the inverse methodology

The estimations of the yield stress in Table 3 were validated against the experimental results of the hardness of the series II nanolaminates, in which the Al and SiC layer thicknesses were equal. To this end, the hardness was computed for the series II nanolaminates using the values of the Al yield stress determined form series I (Table 3). The experimental results and the numerical predictions are plotted in Figure 8, and they show an excellent agreement when the nominal layer thickness was ≥25 nm at 25, 50 and 100 °C, supporting the validity of the inverse methodology and the hypothesis made in this thickness range. Nevertheless, the numerical predictions overestimated the experimental hardness in the case of the thinnest nanolaminates (Al10SiC10) in the whole temperature range. The origin of this discrepancy is not obvious and several hypotheses are currently under investigation. For instance, the

Table 3. Al yield stress as a function of the Al layer thickness and temperature, as determined by applying the inverse methodology to the experimental hardness of the nanolaminates in series I (constant SiC layer thickness).

h_{Al} (nm)	Yield stress (25 °C) (MPa)	Yield stress (50 °C) (MPa)	Yield stress (100 °C) (MPa)
10	1477 ± 39	1280 ± 133	569 ± 39
21	1243 ± 206	877 ± 79	100 ± 38
52	877 ± 64	714 ± 64	190 ± 79
90	891 ± 140	803 ± 140	415 ± 98

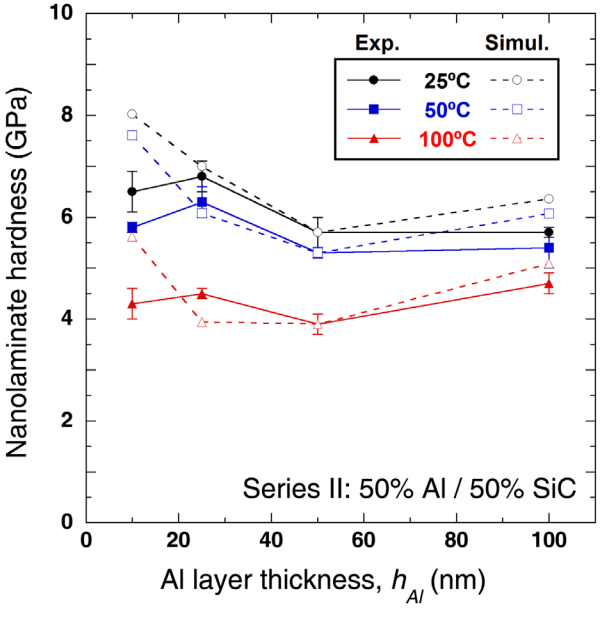

Figure 8. (colour online) Validation of the inverse methodology by comparing the experimental results and the numerical predictions of the hardness for series II nanolaminates at 25, 50 and 100 °C. A good correlation is found between experiments and predictions for layer thickness above 25 nm.

layered structure of the Al10SiC10 could break down in some areas due to the small layer dimensions and the layer waviness, although the limited information provided by the TEM images of Figure 1(e) does not support this assumption. It is also possible that the thickness of the SiC layers is not enough to constrain the deformation of the Al layers and/or that the assumption of a perfectly bonded interface does not hold anymore with such a large interface density.

5. Al deformation mechanism as a function of layer thickness and temperature

5.1. Layer thickness

The values of the yield stress of the Al layers obtained from the inverse methodology are plotted as a function of the Al layer thickness at different temperatures in Figure 9(a). The results of the inverse methodology for layers with 10 nm in thickness were not included, as they could not be validated against the experimental results of the series II nanolaminates.

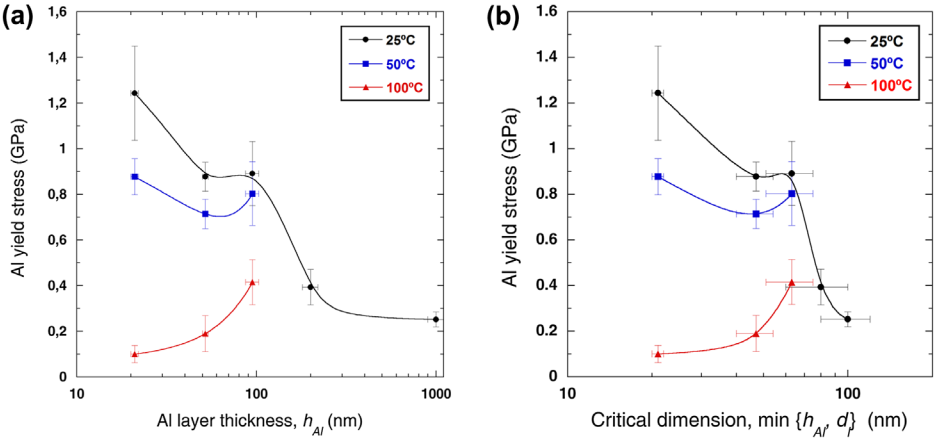

Figure 9. (colour online) Evolution of the Al yield stress at 25, 50 and 100 °C as a function of (a) Al layer thickness, h_{Al}. (b) Minimum of Al layer thickness, h_{Al}, and lateral grain size, d_l. The solid curves are added as guides to the eyes.

The experimental values of the yield stress of monolithic Al films of 1000 and 200 nm in thickness [23], estimated from the room temperature nanoindentation hardness (assuming a Tabor factor of 2.7), were included in this figure for reference. The first interesting observation in this figure is the inversion of the size effect with temperature. While 'the thinner, the stronger' holds at ambient temperature, the mechanical response at 100 °C shows the opposite behavior with 'the thicker, the stronger' and the size effect is not found at 50 °C. The second observation is that the layer thickness was not the only controlling length scale as the 50 and 100 nm thick Al layers displayed identical yield stress, despite the difference in layer thickness. According to the microstructural characterization, the lateral grain size, d_l, became smaller than h_{Al} when the layer thickness reached 100 nm, and this feature should also play a role, as grain boundaries will also act as obstacles to dislocation glide. To account for this, the yield stress was plotted in Figure 9(b) as a function of the critical dimension, understood as the minimum between the layer thickness, h_{Al}, and the lateral grain size, d_l. This new representation of the data provides a clearer picture of the influence of the critical dimension (either layer thickness, h_{Al}, or lateral grain size, d_l) on the yield stress of the Al layers.

The room temperature results for the yield stress of Al layers with thickness in the range 25 to 100 nm showed the expected 'the thinner, the stronger' size effect. In this size range, the Al yield stress is expected to be controlled either by the pile-up of dislocations at interfaces or grain boundaries [42,43], by the CLS of single dislocations [14,44] and/or by the activation of dislocation sources [45]. In the first scenario, the yield stress σ_y is expected to follow a Hall–Petch behavior according to:

$$\sigma_y = \sigma_0 + kl^{-0.5} \tag{1}$$

where l stands for the mean free path of dislocations, σ_0 is the bulk yield stress and k is the Hall–Petch coefficient. Using the values in the literature for pure Al (σ_0 = 10–20 MPa and k = 0.07 MPa $\sqrt{\text{m}}$ [46]), the predictions of Equation (1) with $l = h_{Al}$ underestimated by a large extent the experimental values, Figure 10(a). If $l = \min\{h_{Al}, d_l\}$, the predictions of Equation

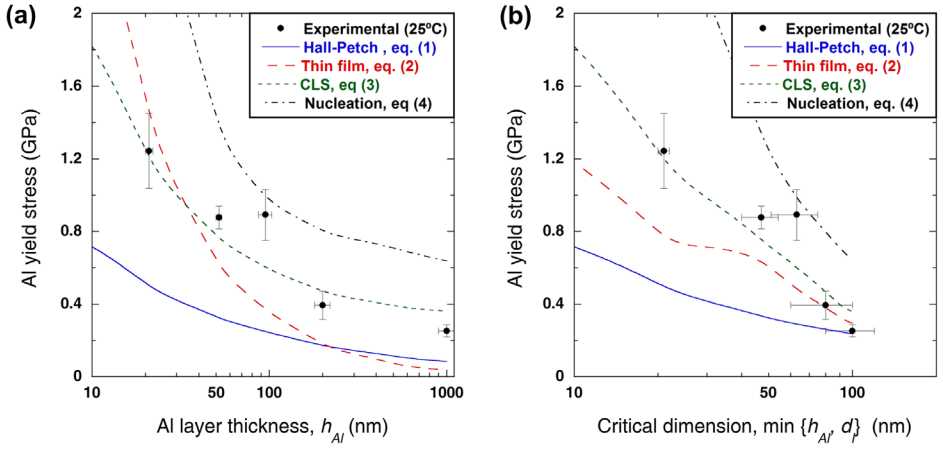

Figure 10. (colour online) Comparison between experiments and predictions of different models for the yield stress at room temperature when the critical distance controlling plastic deformation is: (a) the layer thickness, h_{Al}, and (b) The minimum between the layer thickness, h_{Al}, and the lateral grain size, d_l. Data on thick 1 and 2 μm thick Al layers is taken from Ref. [23].

(1) are closer to the experimental results but still underestimate the experimental data, Figure 10(b). These results are not surprising since it is well established that the mechanics of thin films is substantially different from that of polycrystalline metals.

Nix [42], for single-crystalline thin-films, and later Thomson [43], for polycrystalline films, proposed different expressions accounting for the hardening due to the deposition of dislocation segments at the interfaces and grain boundaries in passivated thin-films. They can be combined in the following simplified equation:

$$\sigma_y = M\frac{Gb}{8\pi(1-\nu)}\left[\frac{1}{t}\ln\left(\frac{t}{b}\right)+\frac{4}{d}\ln\left(\frac{d}{b}\right)\right] \tag{2}$$

where M is the Taylor factor, G and ν are the shear modulus and the Poisson's ratio, respectively, b the Burgers vector, t the film thickness and d the grain size. The work of Nix [42] and Thomson [43] was the first to propose a $1/d$ dependency of the yield stress with film thickness and grain size for thin-films, instead of the $1/d^{0.5}$ dependency coming from the classical Hall–Petch theory. If $M = 3.1$ for an untextured film, and using the constants of Al ($G = 24$ GPa, $\nu = 0.3$, and $b = 0.286$ nm), the predictions of Equation (2) are compared with the experimental results in Figure 10(a) assuming $t = d = h_{Al}$ and in Figure 10(b) assuming $t = h_{Al}$ and $d = d_l$. The variation in the curvature of the curve plotted in Figure 10(b) is due to changes in the aspect ratio of the grains around 50 nm, as indicated above. The qualitative agreement between the predictions of Equation (2) and the experimental data in Figure 10(b) is remarkable for sub-micrometer thick layers but the yield stress of the layers with thicknesses <100 nm was still underestimated.

Strengthening in ultra-thin films has also been explained by the CLS of single dislocations constraint by the presence of impenetrable interfaces [14, 44, 46]. In this case, the stress required for dislocation glide inside one of the Al layers can be expressed as [14]

$$\sigma_y = M\frac{Gb}{8\pi}\left(\frac{4-\nu}{1-\nu}\right)\frac{1}{t}\ln\left(\frac{at}{b}\right)-\frac{f}{t}+\frac{Gb}{L(1-\nu)} \tag{3}$$

where α is the dislocation core cut-off parameter, L the mean spacing of glide loops in a parallel array within the layer, f the characteristic amorphous/crystalline interface stress and the remaining parameters in Equation (3) were defined above. The predictions of Equation (3) using $\alpha = 1$, $L = 30$ nm and $f = 1$ J/m^2 (which are sensible values for this nanocrystalline/amorphous multilayer) and the elastic properties of Al are plotted in Figures 10(a) and (b) and they are in very good agreement with the experimental data. Nevertheless, it should be noted that the predictions of Equation (3) do not depend explicitly on grain size. And, in addition, it is unlikely that CLS is the mechanism controlling strength for layer thicknesses of 100 nm and above when the lateral grain size is smaller than the layer thickness.

Finally, the yield stress may be controlled by the activation of dislocation sources within the Al grains if dislocations are scarce [45,47,48]. The stress necessary to activate dislocation sources according to von Blanckenhagen et al. [45] is given by

$$\sigma_y = M\frac{Gb}{s/4} \tag{4}$$

where s is the smallest between the grain size and the layer thickness, and $s/4$ is an estimate of the most effective dislocation source length that might be contained within one grain. The predictions of Equation (4) are plotted in Figures 10(a) and (b) assuming $s = h_{Al}$ and $s = \min\{h_{Al}, g_l\}$, respectively. Both predictions overestimate the experimental values of the yield stress to a large extent, indicating that the plastic deformation of the nanolayered films is not controlled by the nucleation of new dislocations, and that the presence of pre-existing dislocations leads to yielding at lower stresses. Nucleation of partial dislocations at grain boundaries has also been suggested for Cu thin-films [49], but it is unlikely in the present case because of the high stacking fault energy of Al.

Summing up, these results indicate that the strength of sub-micrometer Al thin-films is controlled by grain boundary strengthening. A transition occurs, however, at 100 nm and plastic deformation becomes controlled by CLS for thinner layers. This change is linked to the aspect ratio of the Al grains, which become wider than the layer thickness at this point. Note that previous works on other metal/ceramic nanolaminate systems, such as Al/Al_2O_3 [15], Al/TiN [16], Ti/TiN [13], suggested the yield stress varied with the layer thickness following Hall-Petch model but no attempt was carried out in these investigations to determine the yield stress of the metallic layers from the nanolaminate strength. Our results point out that it is important to consider other microstructural features, such as the grain size, to get a better understanding of the size effects.

5.2. Temperature

The experimental data presented above showed a dramatic effect of temperature on the mechanical properties of the nanolaminates and on the yield stress of the Al layers (Figure 9). Moreover, the strength reduction increased as the layer thickness decreased, as shown in Figure 11(a) and, as a result, the size effect observed at 25 °C was inverted at 100 °C. The mechanisms controlling the yield stress at room temperature (which were discussed above) only depend on temperature through the elastic constants, and it is obvious that other deformation mechanisms, such as dislocation climb, dislocation cross-slip and/or grain boundary and interface diffusion, have to be triggered at 100 °C to explain the mechanical response. A temperature of 100 °C represents a homologous temperature of ≈0.4 for

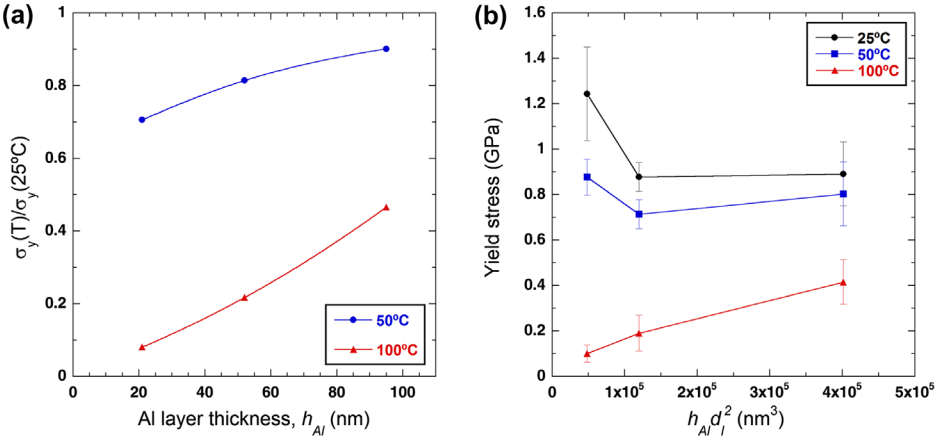

Figure 11. (colour online) (a) Reduction of the yield stress of the Al layers with temperature, $\sigma_y(T)/\sigma_y(25^\circ C)$ as a function of the layer thickness, h_{Al}. (b) Yield stress of the Al layers at 25, 50 and 100 °C vs. $h_{Al}d_l^2$.

Al, which is large enough to trigger diffusion-assisted mechanisms. Considering that the temperature sensitivity is much larger for the thinnest layers, it is instructive to analyze the results based on Coble creep due to grain boundary diffusion. In this case, the strain rate $\dot{\varepsilon}$ can be expressed as [50]

$$\dot{\varepsilon} = A\frac{\sigma}{d^3}\exp\left(\frac{-Q}{RT}\right) \tag{5}$$

where A is a constant that depends on the grain boundary diffusion, R the gas constant, d the grain size and Q the activation energy for grain boundary diffusion. Re-arranging Equation (5), and considering that the grains have a lateral size, d_l and a height, d_v (=h_{Al}), the flow stress can be expressed as,

$$\sigma = \frac{\dot{\varepsilon}}{A}\exp\left(\frac{Q}{RT}\right)d_l^2 h_{Al} \tag{6}$$

and, therefore, should be proportional to the volume of the grains, $d_l^2 h_{Al}$, for a given strain rate and temperature. The dependence of the flow stress with $d_l^2 h_{Al}$ is plotted in Figure 11(b) at 25, 50 and 100 °C. Although this analysis can only be considered as indicative, the results at 100 °C are in very good agreement with the behavior expected for Coble creep and support the hypothesis that interface and grain boundary diffusion might limit the potential strengthening obtained by reducing the thickness of the Al layer at temperatures as low as 100 °C. These results contrast with those obtained in Cu/Nb nanolaminates, that show that strengthening due to size effects is still operative at temperatures as high as 300 °C [4], which also represents an homologous temperature of ≈0.4 for Cu. So, either the behavior of the Cu/Nb interfaces at high temperature differs from that of the Al/SiC interfaces or the high temperature stability of ultra-thin Cu films is larger than that of Al.

6. Conclusions

The mechanical properties of Al/SiC nanolaminates manufactured by magnetron sputtering with layer thicknesses between 10 and 100 nm were studied by nanoindentation in the temperature range 25 to 100 °C. The nanolaminate hardness at 25 °C decreased linearly with the volume fraction of Al and increased non-linearly as the thickness of the Al layers decreased. The nanolaminate showed a dramatic reduction in strength at 100 °C, which was more marked when the Al layers were thinner.

Assuming that the strength of the SiC layers was constant, the strength of the Al layers as a function of the layer thickness and temperature was obtained from the hardness of the nanolaminates by an inverse methodology based on the numerical simulation of the nanoindentation tests using the finite element model. The yield stress of the Al layers at 25 °C showed a large 'the thinner, the stronger' size effect, which depended not only in the layer thickness but also on the microstructure, which changed with the Al layer thickness, h_{Al}. It was found that the vertical grain size, d_v, was always equal to h_{Al}, regardless of the layer thickness but the lateral grain size, d_l, was longer than h_{Al} for layer thicknesses below 50 nm and shorter than h_{Al} for layer thicknesses above 50 nm. Taking these features into account, the yield stress of the Al layers was compatible with a deformation mechanism controlled by the interaction of dislocations with grain boundaries for the thicker layers (>50 nm), while CLS controlled the deformation for layers below 50 nm.

The dramatic reduction in the Al yield strength with temperature, which increased as the Al layer thickness decreased, led to an inverse size effect at 100 °C. The yield stress of the Al in the nanolaminate with 100 nm thick layers was four times higher than that of the nanolaminate with 25 nm thick ones at 100 °C. These results were compatible with plastic deformation mechanisms controlled by grain boundary and interface diffusion at 100 °C, which limit the strength of the ultra-thin Al layers at high temperature.

Acknowledgements

This work was performed, in part, at the Center for Integrated Nanotechnologies, an Office of Science User Facility operated for the U.S. Department of Energy (DOE) Office of Science by Los Alamos National Laboratory (Contract DE-AC52-06NA25396). We thank the assistance of J.K. Baldwin at LANL on the deposition of the multilayers. Authors acknowledge the ICTS-CNME for offering access to their TEM instruments and expertise.

Disclosure statement

No potential conflict of interest was reported by the authors.

Funding

This investigation was supported by the U.S. National Science Foundation (Dr. Lynnette Madsedn, NSF-DMR-1209988) and the Spanish Ministry of Economy and Competitiveness [projects PCIN-2013-029 and MAT2012-31889] under the Materials World Network Program through the project 'High temperature mechanical behavior of metal/ceramic nanolaminate composites'. The multilayer deposition work at LANL was supported by US DOE, Office of Basic Energy Sciences. The financial support from the Chinese Scholarship Council (CSC) (LWY) and of the Spanish Ministry of Education and the Fulbright program (JMMA) are also gratefully acknowledged.

ORCID

J. M. Molina-Aldareguía http://orcid.org/0000-0003-3508-6003

References

[1] I.J. Beyerlein, N.A. Mara, J.S. Carpenter, T. Nizolek, W.M. Mook, T.A. Wynn, R.J. McCabe, J.R. Mayeur, K. Kang, S. Zheng, J. Wang, and T.M. Pollock, *Interface-driven microstructure development and ultra high strength of bulk nanostructured Cu–Nb multilayers fabricated by severe plastic deformation*, J. Mater. Res. 28 (2013), pp. 1799–1812.

[2] J.M. Wheeler, R. Raghavan, V. Chawla, J. Zechner, I. Utke, and J. Michler, *Failure mechanisms in metal–metal nanolaminates at elevated temperatures: Microcompression of Cu–W multilayers*, Scr. Mater. 98 (2015), pp. 28–31.

[3] Y. Kim, A.S. Budiman, J.K. Baldwin, N.A. Mara, A. Misra, and S.M. Han, *Microcompression study of Al–Nb nanoscale multilayers*, J. Mater. Res. 27 (2012), pp. 592–598.

[4] M.A. Monclús, S.J. Zheng, J.R. Mayeur, I.J. Beyerlein, N.A. Mara, T. Polcar, J. Llorca, and J.M. Molina-Aldareguía, *Optimum high temperature strength of two-dimensional nanocomposites*, APL Mater. 1 (2013), p. 052103.

[5] J.H. Lee, W.M. Kim, T.S. Lee, M.K. Chung, B.K. Cheong, and S.G. Kim, *Mechanical and adhesion properties of Al/AlN multilayered thin films*, Surf. Coat. Technol. 133–134 (2000), pp. 220–226.

[6] N.A. Mara, D. Bhattacharyya, P. Dickerson, R.G. Hoagland, and A. Misra, *Deformability of ultrahigh strength 5 nm Cu/Nb nanolayered composites*, Appl. Phys. Lett. 92 (2008), Article ID 231901.

[7] W. Guo, E. Jägle, J. Yao, V. Maier, S. Korte-Kerzel, J.M. Schneider, and D. Raabe, *Intrinsic and extrinsic size effects in the deformation of amorphous CuZr/nanocrystalline Cu nanolaminates*, Acta Mater. 80 (2014), pp. 94–106.

[8] J.Y. Zhang, S. Lei, Y. Liu, J.J. Niu, Y. Chen, G. Liu, X. Zhang, and J. Sun, *Length scale-dependent deformation behavior of nanolayered Cu/Zr micropillars*, Acta Mater. 60 (2012), pp. 1610–1622.

[9] W.Z. Han, A. Misra, N.A. Mara, T.C. Germann, J.K. Baldwin, T. Shimada, and S.N. Luo, *Role of interfaces in shock-induced plasticity in Cu/Nb nanolaminates*, Philos. Mag. 91 (2011), pp. 4172–4185.

[10] I. Knorr, N.M. Cordero, E.T. Lilleodden, and C.A. Volkert, *Mechanical behavior of nanoscale Cu/PdSi multilayers*, Acta Mater. 61 (2013), pp. 4984–4995.

[11] M.A. Monclús, M. Karlik, M. Callisti, E. Frutos, J. LLorca, T. Polcar, and J.M. Molina-Aldareguía, *Microstructure and mechanical properties of physical vapor deposited Cu/W nanoscale multilayers: Influence of layer thickness and temperature*, Thin Solid Films. 571 (2014), pp. 275–282.

[12] D. Bhattacharyya, N.A. Mara, P. Dickerson, R.G. Hoagland, and A. Misra, *Compressive flow behavior of Al–TiN multilayers at nanometer scale layer thickness*, Acta Mater. 59 (2011), pp. 3804–3816.

[13] M.B. Daia, P. Aubert, S. Labdi, C. Sant, F.A. Sadi, P. Houdy, and J.L. Bozet, *Nanoindentation investigation of Ti/TiN multilayers films*, J. Appl. Phys. 87 (2000), pp. 7753–7757.

[14] A. Misra, J.P. Hirth, and R.G. Hoagland, *Length-scale-dependent deformation mechanisms in incoherent metallic multilayered composites*, Acta Mater. 53 (2005), pp. 4817–4824.

[15] A.T. Alpas, J.D. Embury, D.A. Hardwick, and R.W. Springer, *The mechanical properties of laminated microscale composites of Al/Al2O3*, J. Mater. Sci. 25 (1990), pp. 1603–1609.

[16] D. Bhattacharyya, N.A. Mara, R.G. Hoagland, and A. Misra, *Nanoindentation and microstructural studies of Al/TiN multilayers with unequal volume fractions*, Scr. Mater. 58 (2008), pp. 981–984.

[17] X.Y. Zhu, J.T. Luo, F. Zeng, and F. Pan, *Microstructure and ultrahigh strength of nanoscale Cu/Nb multilayers*, Thin Solid Films. 520 (2011), pp. 818–823.

[18] N. Li, J. Wang, A. Misra, and J.Y. Huang, Direct observations of confined layer slip in Cu/Nb multilayers, Microsc. Microanal. 18 (2012), pp. 1155–1162.

[19] J.W. Yan and G.P. Zhang, *Revealing the tunable twinning/detwinning behavior in 25 nm Cu/Au multilayers*, Appl. Phys. Lett. 102 (2013), pp. 86–90.

[20] H.M. Zbib, C.T. Overman, F. Akasheh, and D. Bahr, *Analysis of plastic deformation in nanoscale metallic multilayers with coherent and incoherent interfaces*, Int. J. Plast. 27 (2011), pp. 1618–1639.
[21] N. Abdolrahim, H.M. Zbib, and D.F. Bahr, *Multiscale modeling and simulation of deformation in nanoscale metallic multilayer systems*, Int. J. Plast. 52 (2014), pp. 33–50.
[22] N. Chawla, D.R.P. Singh, Y.-L. Shen, G. Tang, and K.K. Chawla, *Indentation mechanics and fracture behavior of metal/ceramic nanolaminate composites*, J. Mater. Sci. 43 (2008), pp. 4383–4390.
[23] X. Deng, N. Chawla, K.K. Chawla, M. Koopman, and J.P. Chu, *Mechanical behavior of multilayered nanoscale metal-ceramic composites*, Adv. Eng. Mater. 7 (2005), pp. 1099–1108.
[24] D.R.P. Singh, N. Chawla, G. Tang, and Y.-L. Shen, *Micropillar compression of Al/SiC nanolaminates*, Acta Mater. 58 (2010), pp. 6628–6636.
[25] G. Tang, Y.-L. Shen, D.R.P. Singh, and N. Chawla, *Indentation behavior of metal–ceramic multilayers at the nanoscale: Numerical analysis and experimental verification*, Acta Mater. 58 (2010), pp. 2033–2044.
[26] S. Lotfian, M. Rodríguez, K.E. Yazzie, N. Chawla, J. Llorca, and J.M. Molina-Aldareguía, *High temperature micropillar compression of Al/SiC nanolaminates*, Acta Mater. 61 (2013), pp. 4439–4451.
[27] S. Lotfian, J.M. Molina-Aldareguia, K.E. Yazzie, J. Llorca, and N. Chawla, *High-temperature nanoindentation behavior of Al/SiC multilayers*, Philos. Mag. Lett. 92 (2012), pp. 362–367.
[28] M.A. Monclús, S. Lotfian, and J.M. Molina-Aldareguía, *Tip shape effect on hot nanoindentation hardness and modulus measurements*, Int. J. Precis. Eng. Manuf. 15 (2014), pp. 1513–1519.
[29] C. Mayer, N. Li, N. Mara, and N. Chawla, *Micromechanical and in situ shear testing of Al–SiC nanolaminate composites in a transmission electron microscope (TEM)*, Mater. Sci. Eng., A. 621 (2015), pp. 229–235.
[30] Y.L. Shen, C.B. Blada, J.J. Williams, and N. Chawla, *Cyclic indentation behavior of metal–ceramic nanolayered composites*, Mater. Sci. Eng., A. 557 (2012), pp. 119–125.
[31] S. Lotfian, C. Mayer, N. Chawla, J. Llorca, A. Misra, J.K. Baldwin, and J.M. Molina-Aldareguía, *Effect of layer thickness on the high temperature mechanical properties of Al/SiC nanolaminates*, Thin Solid Films. 571 (2014), pp. 260–267.
[32] J. Llorca, A. Needleman, and S. Suresh, *An analysis of the effects of matrix void growth on deformation and ductility in metal-ceramic composites*, Acta Metall. Mater. 39 (1991), pp. 2317–2335.
[33] J. Llorca and C. González, *Microstructural factors controlling the strength and ductility of particle-reinforced metal-matrix composites*, J. Mech. Phys. Solids. 46 (1998), pp. 1–28.
[34] M.D. Gram, J.S. Carpenter, and P.M. Anderson, *An indentation-based method to determine constituent strengths within nanolayered composites*, Acta Mater. 92 (2015), pp. 255–264.
[35] W.C. Oliver and G.M. Pharr, *An improved technique for determining hardness and elastic modulus using load and displacement sensing indentation experiments*, J. Mater. Res. 7 (1992), pp. 1564–1583.
[36] K.K. Shih and D.B. Dove, *Ti/Ti-N Hf/Hf-N and W/W-N multilayer films with high mechanical hardness*, Appl. Phys. Lett. 61 (1992), pp. 654–656.
[37] P.L. Sun, J.P. Chu, T.Y. Lin, Y.L. Shen, and N. Chawla, *Characterization of nanoindentation damage in metal/ceramic multilayered films by transmission electron microscopy (TEM)*, Mater. Sci. Eng., A. 527 (2010), pp. 2985–2992.
[38] N.A. Mara, N. Li, A. Misra, and J. Wang, *Interface-driven plasticity in metal-ceramic nanolayered composites: Direct validation of multiscale deformation modeling via in situ indentation in TEM*, JOM. 68 (2016), pp. 143–150.
[39] A.C. Fischer-Cripps, The IBIS Handbook of Nanoindentation, Fischer-Cripps Laboratories, Forestville, NSW, 2009.
[40] R.D. Jamison and Y.-L. Shen, *Indentation behavior of multilayered thin films: Effects of layer undulation*, Thin Solid Films. 570 (2014), pp. 235–242.
[41] C. Mayer, L.W. Yang, S.S. Singh, H. Xie, Y.-L. Shen, J. Llorca, J.M. Molina-Aldareguia, and N. Chawla, *Orientation dependence of indentation behavior in Al–SiC nanolaminate composites*, Mater. Lett. 168 (2016), pp. 129–133.

[42] W. Nix, *Mechanical properties of thin films*, Metall. Trans. A. 20 (1989), pp. 2217–2245.
[43] C.V. Thompson, *The yield stress of polycrystalline thin films*, J. Mater. Res. 8 (1993), pp. 1992–1993.
[44] W.D. Nix, *Yielding and strain hardening of thin metal films on substrates*, Scr. Mater. 39 (1998), pp. 545–554.
[45] B.V. von Blanckenhagen, P. Gumbsch, and E. Arzt, *Dislocation sources and the flow stress of polycrystalline thin metal films*, Philos. Mag. Lett. 83 (2003), pp. 1–8.
[46] M. Phillips, B. Clemens, and W. Nix, *Microstructure and nanoindentation hardness of Al/Al3Sc multilayers*, Acta Mater. 51 (2003), pp. 3171–3184.
[47] G. Dehm, D. Weiss, and E. Arzt, *In situ transmission electron microscopy study of thermal-stress-induced dislocations in a thin Cu film constrained by a Si substrate*, Mater. Sci. Eng., A. 309–310 (2001), pp. 468–472.
[48] R. Raghavan, T.P. Harzer, V. Chawla, S. Djaziri, B. Phillipi, J. Wehrs, J.M. Wheeler, J. Michler, and G. Dehm, *Comparing small scale plasticity of copper-chromium nanolayered and alloyed thin films at elevated temperatures*, Acta Mater. 93 (2015), pp. 175–186.
[49] A.G. Patric, B. Jochen, O. Felix, W. Alexander, S. Ralph, and A. Eduard, *Size effects on yield strength and strain hardening for ultra-thin Cu films with and without passivation: A study by synchrotron and bulge test techniques*, Acta Mater. 56 (2008), pp. 2318–2335.
[50] R.L. Coble, *A model for boundary diffusion controlled creep in polycrystalline materials*, J. Appl. Phys. 34 (1963), pp. 1679–1682.